Title
Chemical genetic discovery of targets and anti-targets for cancer polypharmacology

Journal
Nature, 486(7401)

ISSN
0028-0836

Authors
Dar, Arvin C
Das, Tirtha K
Shokat, Kevan M
et al.

Publication Date
2012-06-01

DOI
10.1038/nature11127

Peer reviewed

Published in final edited form as:
Nature. ; 486(7401): 80–84. doi:10.1038/nature11127.

Chemical genetic discovery of targets and anti-targets for cancer polypharmacology

Arvin C. Dar[1,*], **Tirtha K. Das**[2,*], **Kevan M. Shokat**[1], and **Ross L. Cagan**[2]

[1]Howard Hughes Medical Institute and Department of Cellular and Molecular Pharmacology, University of California, San Francisco, California 94158, USA

[2]Department of Developmental and Regenerative Biology, Mount Sinai School of Medicine, New York, New York 10029, USA

Abstract

The complexity of cancer has led to recent interest in polypharmacological approaches for developing kinase-inhibitor drugs; however, optimal kinase-inhibition profiles remain difficult to predict. Using a Ret-kinase-driven *Drosophila* model of multiple endocrine neoplasia type 2 and kinome-wide drug profiling, here we identify that AD57 rescues oncogenic Ret-induced lethality, whereas related Ret inhibitors imparted reduced efficacy and enhanced toxicity. *Drosophila* genetics and compound profiling defined three pathways accounting for the mechanistic basis of efficacy and dose-limiting toxicity. Inhibition of Ret plus Raf, Src and S6K was required for optimal animal survival, whereas inhibition of the 'anti-target' Tor led to toxicity owing to release of negative feedback. Rational synthetic tailoring to eliminate Tor binding afforded AD80 and AD81, compounds featuring balanced pathway inhibition, improved efficacy and low toxicity in *Drosophila* and mammalian multiple endocrine neoplasia type 2 models. Combining kinase-focused chemistry, kinome-wide profiling and *Drosophila* genetics provides a powerful systems pharmacology approach towards developing compounds with a maximal therapeutic index.

The cellular kinase-signalling network is a major regulator of cancer progression. Kinase-signalling pathways are often involved in pathogenesis, and kinase mutations are common and potent drivers of oncogenesis[1–4]. Targeting a single kinase has proven successful in some cases; examples include drugs that inhibit BCR–ABL, as well as members of the EGFR and RAF class of proteins[5–7]. However, results of this approach have been mixed[8–10]. Difficulties include rapidly emerging resistance as well as considerable toxicity that can limit dosing to levels that are insufficient for blocking tumour growth.

By contrast, most drugs approved for clinical use have multiple targets[11–13]. For many, or perhaps most, 'off-target' activities contribute to the overall efficacy of a drug. Sorafenib provides a recent example[14]: it was developed initially as an inhibitor of RAF kinase, but its

Correspondence and requests for materials should be addressed to K.M.S. (shokat@cmp.ucsf.edu).
*These authors contributed equally to this work.

Supplementary Information is linked to the online version of the paper at www.nature.com/nature.

Author Contributions A.C.D. and T.K.D. contributed equally and are listed alphabetically. A.C.D. and T.K.D. conceived and designed experiments with K.M.S. and R.C. A.C.D. performed chemical synthesis, modelling, IC_{50} measurements, informatics and western blots on cancer cell lines. T.K.D. performed, imaged and analysed all *Drosophila* assays and cancer cell line viability assays. All authors discussed experimental data and wrote the manuscript.

Author Information Reprints and permissions information is available at www.nature.com/reprints. The authors declare competing financial interests: details accompany the full-text HTML version of the paper at www.nature.com/nature. Readers are welcome to comment on the online version of this article at www.nature.com/nature

efficacy in renal and hepatocellular cancer was later attributed to inhibition of VEGFR2 and PDGFR and potentially other targets[15]. Sorafenib highlights the therapeutic potential of targeting multiple kinases but also the uncertainty and serendipity of phenotype-based screening.

Most multiple endocrine neoplasia type 2 (MEN2) patients have an autosomal-dominant activating germline mutation in the RET (rearranged during transfection) receptor tyrosine kinase that is necessary and probably sufficient to direct a series of transformation events including medullary thyroid carcinoma (MTC)[16,17]. To identify candidate compounds with optimal polypharmacological profiles, we synthesized a panel of inhibitors with potency against RET (a traditional target-based approach) that additionally target distinct downstream kinases. We demonstrate how stepwise testing in *Drosophila* models of the disease subtype MEN2B[18] uncovered a spectrum of targets contributing to drug-induced efficacy and toxicity. Our results present a new approach to rational drug development that combines aspects of target- and phenotype-based drug discovery; it relies on whole-animal screening to both explore the mechanism of a drug and identify an optimal polypharmacological profile for suppressing tumours *in vivo*.

Identifying AD57 in a whole-animal *Drosophila* screen

We previously reported a *Drosophila* MEN2B model in which an activating intracellular mutated isoform of the *Drosophila* Ret orthologue (dRet) was targeted to the eye[18]. This $dRet^{MEN2B}$ model proved useful for validating whole-animal efficacy of the kinase inhibitor vandetanib (also known as ZD6474, Caprelsa)[19], a drug recently approved for sporadic MTC and for MTC arising in patients with MEN2 (ref. 20). To improve its utility for drug screening, we developed a quantitative viability assay that uses the GAL4/upstream activating system (UAS) to target oncogenic $dRet^{MEN2B}$ to multiple developing epithelial tissues (Fig. 1a; T.K.D. *et al.*, in preparation). Specifically, oncogene expression is driven by the *patched* (*ptc*) promoter, which directs expression in a dynamic pattern including developing epithelia (for example, wing, eye and leg) and other tissues[21]. We calibrated the $ptc>dRet^{MEN2B}$ assay to permit 50% survival to pupariation and 0% survival to adulthood. Oral administration of clinical kinase inhibitors[22,23] resulted in weak (vandetanib), mild (sunitinib) or stronger (sorafenib) rescue (Fig. 1b), validating our assay. Notably, sorafenib rescued some animals to adulthood but did not considerably increase the proportion that developed to pupariation, indicating some efficacy but also toxicity (reduced survival) at optimal doses.

We developed and screened a library of polypharmacological compounds that target Ret in addition to other classes of kinases[24] (Supplementary fig. 1). One compound, AD57, potently suppressed $ptc > dRet^{MEN2B}$ lethality in the larva, rescuing approximately 25% of animals to adulthood (Fig. 1b, c). Rescued adults also showed complete suppression of notum and scutellum defects that were observed in un-eclosed control pupae (Fig. 1c), and were fully active and fertile. AD57 demonstrated both an improved efficacy and toxicity profile in our assay compared with other kinase inhibitors (Fig. 1b).

AD57 exhibited improved activity compared to analogues

The overall structure of AD57-like compounds includes two fragments fused through a urea linker (Fig. 1d). Shared features include a pyrazolopyrimidine core that functions as a mimic of adenosine or hinge-binder and a hydrophobic element that binds within an allosteric pocket of the kinase domain (Supplementary Fig. 1b). AD36, a close analogue of AD57, contains a methylene group between the pyrazolopyrimidine ring and fused phenyl portion, whereas the analogue AD58 does not contain the trifluoromethyl group (Fig. 1d). These subtle structural changes led to substantial changes in biological activity; AD36 showed

some efficacy (increased numbers of pupae but no adults), whereas AD58 induced considerable toxicity without detectable efficacy (fewer pupae and adults; Fig. 1b).

These results demonstrate the sensitivity of whole-body phenotyping in *Drosophila* to detect the effects of conservative structural differences between drug candidates. The difference between AD36 and AD57 was particularly notable because both demonstrate similar potency for Ret *in vitro* (Fig. 1d); indeed, our analysis of other kinase inhibitors indicated that efficacy did not correlate solely with inhibition of Ret (Fig. 2c and Supplementary Fig. 2; data not shown). This suggested that targeting of additional kinases is necessary for the biological efficacy of AD57.

AD57 suppressed *dRet^{MEN2}* transformation

We previously developed a wing-based assay for transformation and cell migration in which the *ptc-Gal4* driver directed oncogene expression in a stripe along the anterior–posterior axis[25]. Adapting it to *ptc > dRet^{MEN2B}* wings led to overproliferation, basal constriction and cell migration away from the *ptc* domain (Fig. 2a; T.K.D. *et al*, in preparation). Oral administration of AD57 blocked each of these phenotypes (Fig. 2a). Sorafenib, sunitinib and vandetanib showed substantially weaker rescue (Fig. 1b; data not shown). We conclude that oral administration of AD57 is particularly effective at suppressing dRet-mediated transformation at doses that are non-toxic to the fly.

In standard mammalian RET^{MEN2} models, AD57 potently inhibited the viability of MEN2B (MZ-CRC-1) and MEN2A (TT) patient-derived cell lines with a half-maximum inhibitory concentration (IC_{50}) that was several orders more potent than sorafenib, vandetanib, AD36 or AD58 (Supplementary Fig. 3a, b). In a conventional mouse xenograft model, AD57 significantly suppressed TT-based tumour growth at a dose (20 mg kg^{-1}) that demonstrated no detectable toxicity as assessed by animal weights (Supplementary Fig. 3c, d). Together, our data indicate that *Drosophila in vivo* assays provide a useful tool for identifying compounds with improved *in situ* efficacy and toxicity profiles.

Erk and Src inhibition suppressed dRet signalling

Our previous *Drosophila* genetic screens emphasized three major pathways for dRet^{MEN2B}-mediated transformation: Ras/Raf, Src and glucose metabolism/PI3K[18] (Fig. 2b; data not shown). Furthermore, assessing AD57, AD36 and AD58 in a broad *in vitro* mammalian-kinase panel indicated that small perturbations in the structure of AD57 led to considerable changes in kinase selectivity (Fig. 1e and Supplementary Tables 1–3). For example, AD57 is a potent inhibitor of the pathway-relevant human kinases BRAF, S6K (also known as RPS6KB1),mTORand SRC (Fig. 2c). By comparison, AD58 is a much weaker inhibitor of S6K and BRAF but is more potent against mTOR; AD36 is nearly inactive against mTOR, S6K and SRC, potentially reflecting steric clash at the gatekeeper position (compare, for example, ABL(T315I), EGFR(T790M) and RET(V804L); Supplementary Fig. 4). We focused on effectors of RAS, PI3K and SRC, although other targeted pathways may also contribute to compound activity.

We demonstrated previously that activation of Src is sufficient to direct many of the aspects we observed within the *ptc > dRet^{MEN2B}* domain[25–27] and we explored its activity *in situ*. Expressing *ptc > dRet^{MEN2B}* led to high levels of activated phospho-Src at the basal invading front of transformed cells (Fig. 2a). In addition to suppressing invasion, oral administration of AD57 suppressed phospho-Src in basal regions of the wing epithelium (Fig. 2a). Distinctions with AD36 and AD58 were instructive. AD36 failed to suppress the invasion or basal migration of *ptc > dRet^{MEN2B}* cells and, as predicted by our *in vitro* assay, phospho-Src remained at high levels at the basal leading edge (Fig. 2a). Also as predicted,

AD58 suppressed basal phospho-Src accumulation, yet it failed to prevent invasion and basal migration (Fig. 2a). These data support the view that Src inhibition contributes to reducing invasion and basal migration, but suggest that other targets are also required.

Elevated Ras/Erk pathway activity leads to ectopic veins in the adult wing (for example, refs 28, 29). Expression of oncogenic dRet throughout the developing wing (*765 > dRet^{MEN2B}*) led to disruption of the overall adult wing pattern, including ectopic wing veins. Reducing gene dosage of the *erk* orthologue *rolled* suppressed these phenotypes, confirming that wing vein formation is dependent on Ras/Erk activity (Fig. 2d). *dRet^{MEN2B}*-dependent wing phenotypes were suppressed by AD57 (Fig. 2d); by contrast, vandetanib had little effect (Supplementary Fig. 5a, b). Notably, the ectopic wing vein phenotype was slightly but consistently enhanced with AD58 treatment (Fig. 2d). This enhancement was suppressed by removing a functional copy of *erk* (Fig. 2d and Supplementary Fig. 5c), further indicating that AD58 treatment actually increased Ras pathway signalling. These data raise the possibility that AD58 toxicity was due to excess Ras pathway activity and that further suppressing Ras pathway activity would improve the overall efficacy of AD57.

Unbalanced dTor inhibition promotes toxicity

AD58 directed substantial whole-animal toxicity when fed to *ptc > dRet^{MEN2B}* or wild-type flies (Figs 1a, 3a, b and Supplementary Fig. 6), providing us with an opportunity to explore aspects of AD drug-class toxicity. On the basis of *in vitro* kinase data, AD58 is a stronger inhibitor of mTOR and a weaker inhibitor of RAF than AD57 (Fig. 2c and Supplementary Fig. 4c). Recently, mTOR has been demonstrated to provide feedback inhibition of the RAS pathway in mammals[30,31]. We therefore assessed whether the high toxicity observed for AD58 was due in part to high inhibition of Drosophila target of rapamycin (dTor) coupled with low inhibition of Raf, leading to hyperactivation of *Drosophila* Ras85D pathway signalling throughout the animal.

Reducing dTor (*ptc > dRet^{MEN2B}*, *dTor$^{-/+}$*) dominantly suppressed the efficacy of AD57 and enhanced the toxicity of AD58 (Fig. 3a). Quantitative phenotypic assessment indicated that AD58-induced toxicity was due primarily to an increase in proliferation (Fig. 3c, e). Also, reducing the gene dosage of *dTor* enhanced the AD58-induced ectopic wing vein formation (Fig. 3d) and suppressed efficacy of AD57 on wing vein patterning (Supplementary Fig. 5b), indicating that reducing dTor increased Erk activity. Notably, removing a genomic copy of the dTor target S6K suppressed AD58 toxicity (Fig. 3a), indicating that S6K is independent of the dTor feedback loop.

We also assessed whether reducing the activity of *Drosophila* Ras85D pathway components could abrogate the effects of dTor inhibition. AD58-mediated toxicity in wild-type flies was almost completely suppressed by co-feeding with the Raf inhibitor sorafenib or Mek inhibitor AZD6244 (Fig. 3b). Combining AD58 with sorafenib also resulted in considerable suppression of invasion and migration within *ptc > dRet^{MEN2B}* wing discs (Fig. 3f). Removing a genomic copy of *erk/rolled* considerably improved AD57 rescue (Fig. 3a). Together, these data indicate that both AD57 and AD58 act to inhibit dTor activity, but that failure of AD58 to suppress Raf kinase led to elevated Ras pathway activity. Elevated Erk, in turn, led to poor efficacy against the tumour and high whole-body toxicity (see Fig. 5 for pathway logic).

AD80 and AD81 demonstrated an improved profile

Together, our genetic and chemical data indicate that an optimal drug for MEN2B would show activity against Ret, Src, S6K and Raf but limited activity against Tor. To test this logic and potentially improve AD57, we developed a series of new AD-based analogues.

From our previously determined structure of AD57 in complex with c-Src we reasoned that modifying the terminal phenyl group of AD57 would selectively perturb dTor binding without altering inhibitory interactions with dRet, Raf, S6K or Src. We therefore generated two compounds, AD80 andAD81, into which ortho-fluorine and para-chlorine groups were respectively incorporated (Fig. 4a).

On the basis of their *in vitro* human kinase profiles, AD80 and AD81 inhibited RET, RAF, SRC and S6K, with greatly reduced mTOR activity relative to AD57 and AD58 (Fig. 4a and Supplementary Fig. 7). Oral administration of either AD80 or AD81 resulted in a notable 70–90% of animals developing to adulthood in our *Drosophila ptc > dRet^{MEN2B}* model, a considerable improvement over the efficacy observed with AD57 and all other compounds we have tested until now (Fig. 4b). Focusing on AD80, ectopic Src activation (Fig. 4c) and wing vein pattern phenotypes (Fig. 4e and Supplementary Fig. 6b) were strongly suppressed, indicating that Src and Ras activities were restored to normal levels. The result was phenotypically normal *ptc > dRet^{MEN2B}* adults, showing rescue that exceeded AD57 or sorafenib, which yielded adults with some cuticle defects. Notably, although reducing *erk* gene dosage (*ptc > dRet^{MEN2B}*, *erk*−/+) in the fly considerably enhanced the efficacy of AD57 and AD58 in viability assays, it did not alter efficacy of AD80 treatment (Fig. 4d). This indicates that AD80 is optimal for Ras–Erk pathway inhibition (Supplementary Fig. 2).

The improved profile of AD80 also translated to mammalian MEN2 models. AD80 inhibited proliferation of MZ-CRC-1 and TT thyroid cancer cells in culture, probably through the induction of apoptosis (Supplementary Fig. 8). Immunoblot analysis demonstrated potent downregulation of phosphorylated Ret and several downstream biomarkers within these cells (Supplementary Fig. 9).AD80 also promoted enhanced tumour growth inhibition and reduced body-weight modulation relative to vandetanib in a mouse xenograft model (Fig. 4f, g and Supplementary Table 4).

Discussion

Here we describe a systems pharmacology approach for cancer drug discovery that focuses on whole-animal testing, chemistry and genetics to identify a single agent with an optimized polypharmacological profile. Using a stepwise approach that combined genetics and chemistry, we identified AD80 and AD81 as polypharmacological agents with an optimal balance of activity against Ret, Raf, Src, Tor and S6K that show high efficacy with very low toxicity (Fig. 5). Our studies indicate that these drugs may be an improvement over existing compounds including vandetanib, a kinase inhibitor demonstrated by our group and others to act on Ret-based tumorigenesis[19,32] that has recently been approved for MTC patients. Details of human tumours can differ substantially from *Drosophila* cancer models and mouse xenografts, and the true predictive value of this approach must await further testing. A related approach is to assess drug combinations; however, in addition to the increased cost of clinically testing a mix of compounds, complex target-profile interactions and differing pharmacokinetics can make executing clinical trials challenging.

The connection between the Tor and Ras pathways within the MEN2B model is reminiscent of a general network motif termed an incoherent feed-forward loop[33]: here, dRet^{MEN2B} activates Ras but also represses Ras signalling by activating dTor. This network motif has been identified within diverse contexts, including transcriptional and neuronal networks, as a means to tune cellular responses to incoming signals[33]. Perhaps this motif will prove common within cancer signalling networks, providing a useful place to search for other anti-targets that limit the therapeutic benefits of kinase inhibitors.

METHODS

Inhibitor studies in flies

AZD6244 (Cal Biochem), sorafenib, sunitinib (LC Labs) and new AD-series drugs were dissolved in DMSO buffer and then diluted in molten (~50 °C)-enriched fly food and left to solidify at room temperature (25 °C) to yield the indicated final drug concentrations. 30–60 embryos of each genotype were raised on drug-containing food (500–1,000 μl) in 5-ml vials until they matured as third-instar larvae (wing disc migration and invasion assay) or allowed to proceed to adulthood (viability assay and wing vein quantification assay). Experiments were done in duplicate and repeated at least three times.

Fly stocks, genetics and subcloning

Fly stocks were obtained from Bloomington stock centres and C. Pfleger (*rolled*[1]). *UAS-dRet*^{MEN2B} flies were generated by ligating a partial EcoR1-digested *glass* multimerized repeat–*dRet*^{MEN2B} DNA fragment[18] into EcoR1 site of *pUAST* vector. Transgenic flies were generated by standard protocol.

Histology and antibodies

For wing disc invasion and migration analysis third-instar discs were staged and fixed in 4% paraformaldehyde. Immunofluorescence was performed as described[34]. Antibodies used were anti-phospho-Src(Y^{418}) (Invitrogen). AlexaFluor secondary antibodies were used for all immunofluorescence experiments. Confocal imaging used a Leica DM5500 Q microscope and image analysis was performed using Adobe Photoshop.

MTT assays using cancer lines

MZ-CRC-1 (MEN2B) and TT (MEN2A) cell lines were cultured in DMEM buffer and Ham's F12K media, respectively, supplemented with 10% bovine serum albumin (BSA) and a penicillin and streptomycin antibiotics mix. Cells were grown in 75 cm^2 sterile polystyrene culture flasks to 80% confluency, trypsinized and re-seeded in equal aliquots into 96-well plates. After 2 days and ~50% confluency, media was removed and replaced with DMSO or drug-containing media. Cells were allowed to grow for another 6 days, after which the thiazolyl blue tetrazolium bromide (MTT) assay was performed. Cell media was removed and replaced with MTT-containing media (1 mg ml^{-1} final concentration) and cells were allowed to grow at 37 °C for another 3.5 h. MTT media was removed and MTT precipitate dissolved in 4 mM HCl, 0.1% NP40 in isopropanol, solvent by shaking for 1 h. Spectrophotometric readings at 590 nm and 630 nm using a 96-well-plate reader were used to establish growth and viability of cells. Each drug dose was tested in quadruplicates and experiments repeated twice.

Western blotting of fly wing disc tissues

A total of ten third-instar discs of each treatment were dissolved in lysis buffer (50 mM Tris, 150 mM NaCl, 1% Triton X-100, 1 mM EDTA) supplemented with protease-inhibitor cocktail and phosphatase-inhibitor cocktail (Sigma). Total protein in each sample was quantified using BIORAD protein assay. Samples were boiled, resolved on SDS–PAGE and transferred by standard protocols. Membranes were stripped with SIGMA Restore stripping buffer and re-probed with other antibodies to assess the signal under exactly the same loading conditions. Antibodies used were from Cell Signaling Technology. Only phospho-Src antibody was from Invitrogen.

Whole-mount imaging of fly notum and wings

For fly notum images, after completion of the viability assay, un-eclosed pupae were dissected out of their pupal cases, placed on double-sided tape and imaged under the Leica MZ16F stereomicroscope. Eclosed adults were imaged similarly. For adult wing vein analysis, wings from male flies were dissected and kept in 100% ethanol overnight, mounted on slides in 80% glycerol in phosphate-buffered saline solution and imaged by regular light microscopy using a Leica DM5500 Q microscope.

Xenograft analysis

5×10^6 TT cells were injected subcutaneously into one flank of male *nu nu* mice. Mice showing established growing tumours were separated into vehicle or drug-treatment groups. A similar range of tumour sizes was selected for each experiment (vehicle versus AD57; vehicle versus AD80 versus vandetanib). Vehicle, AD57 (20 mg kg^{-1}), AD80 (30 mg kg^{-1}) or vandetanib (50 mg kg^{-1}) were administered by oral gavage (per os) once daily, five times a week. Tumour and body-weight measurements were performed three times per week. Mouse experiments were carried out by Washington Biotechnology (accreditation no. A192-01) according to the Public Health Services guideline, set forth by the Office for Laboratory and Animal Welfare division of the National Institutes of Health.

Western blotting of cancer cell lines

MZ-CRC-1 (MEN2B) and TT (MEN2A) cell lines were grown in 24-well plates in DMEM buffer (+ 4.5 g l^{-1} glucose; without L-Glu and pyruvate) and Ham's F12K (ATCC) media respectively; each supplemented with 10% heat-inactivated FBS and penicillin and streptomycin antibiotics. Cells were treated for 1 h with inhibitors or vehicle (0.1% DMSO). After treatment, media was removed and cells were washed twice with cold PBS and then lysed in radioimmunoprecipitation assay buffer (25mM Tris, pH 7.6, 150 mM NaCl, 1% NP-40, 0.1% SDS) containing protease and phosphatase inhibitors (Roche). Cell lysates were separated by SDS–PAGE, transferred to nitrocellulose and blotted for the indicated proteins using commercial antibodies (all were from Cell Signaling Technology). For measuring cleaved poly ADP ribose polymerase (PARP) and cleaved caspase 3, cells were treated identically with the following exceptions: cells were incubated with inhibitors for 72 h, causing a number of cells to become non-adherent. Both adherent and non-adherent cells were combined before cell lysis and immunoblot analysis.

IC_{50} value measurements

A recombinant glutathione *S*-transferase (GST)–RET kinase domain fusion (Invitrogen) was diluted in a mix containing phosphor-acceptor peptide (132 μM final concentration; sequence: EAIYAAPFKKK), buffer (10 mM $MgCl_2$, 10 mM HEPES 7.2, 40 ng BSA) and varying concentrations of inhibitor. Reactions were initiated by addition of 100 μM cold ATP supplemented with 5 μCi γ^{32}P-ATP. After 15 min at room temperature, 2 μl of the reactions (out of 25 μl total volume) were spotted onto P81 phosphocellulose paper (Whatman). Blots were washed at least 5 times over 1 h in 1% (v/v) phosphoric acid and blots were then dried and transferred radioactive counts were measured by phosphorimaging using a Typhoon Scanner (Molecular Dynamics). Quantification was conducted with ImageQuant software and titration data were fit to a sigmoidal dose response to derive IC_{50} values in the Prism software package. Inhibitors were diluted threefold over a final concentration range of 0.0005–100 μM to derive dose–response curves. Experiments were completed three times to derive mean and standard error measurements. IC_{50} values for KDR, SRC, ABL, C-RAF, mTOR, EGFR and AKT1 were determined similarly with the following exceptions. Dephosphorylated casein was used as a substrate for mTOR (Invitrogen). Inactive MEK1 (Millipore) was used as a substrate for C-RAF (Millipore).

Poly Glu-Tyr was used as the substrate for KDR (Invitrogen), EGFR (Invitrogen), SRC (purified as previously described[24]) and ABL (purified as previously described[24]). Myelin basic protein was used as a substrate for AKT1 (Invitrogen).

Kinase-inhibitor profiling

AD36, AD57, AD58, AD80 and AD81 were assayed by Invitrogen to derive percentage inhibition of kinase activity. All compounds were screened at 1 μM and values are shown in Supplementary Tables 1–3. Detailed procedures for kinase reactions, ATP concentrations used and Z'-LYTE or Adapta assay formats are described in the SelectScreen Customer Protocol (http://www.invitrogen.com/kinaseprofiling). Kinase-inhibition data for 1 μM inhibitor of each of the clinical and tool compounds staurosporine, sunitinib, dasatinib, pyrazolopyrimidine 2, gefitinib, imatinib, SB202190, erlotinib and BIRB796 were obtained from Invitrogen (http://tools.invitrogen.com/content/sfs/brochures/Activity_Assay_Kinase_Selectivity_Data.pdf). Clustering and visualization were performed with Cluster 3.0 and Java TreeView (http://bonsai.hgc.jp/~mdehoon/software/cluster/software.htm).

Chemical synthesis

The AD compounds were synthesized using a seven-step chemical synthesis that is described in detail in the Supplementary Methods. Final products were characterized by nuclear magnetic resonance spectroscopy and liquid-chromatography–mass spectrometry.

Supplementary Material

Refer to Web version on PubMed Central for supplementary material.

Acknowledgments

We thank the Bloomington Stock Center, Vienna *Drosophila* RNAi Center and C. Pfleger for reagents. T.K.D. and R.C. were supported by National Institutes of Health grants R01CA109730 and R01CA084309 and American Cancer Society Grant 120616-RSGM-11-018-01-CDD. T.K.D. was also supported by American Cancer Society Grant 120886-PFM-11-137-01-DDC. We thank members of the Shokat and Cagan laboratories for discussions. We thank members of the SelectScreen team at Invitrogen, in particular K. Vogel, for performing kinase-profiling services. K.M.S. thanks NIH R01EB001987, P01 CA081403-11 and The Waxman Foundation.

References

1. Ding L, et al. Somatic mutations affect key pathways in lung adenocarcinoma. Nature. 2008; 455:1069–1075. [PubMed: 18948947]
2. Greenman C, et al. Patterns of somatic mutation in human cancer genomes. Nature. 2007; 446:153–158. [PubMed: 17344846]
3. Wood LD, et al. The genomic landscapes of humanbreast and colorectal cancers. Science. 2007; 318:1108–1113. [PubMed: 17932254]
4. Cancer Genome Atlas Research Network. Comprehensive genomic characterization defines human glioblastoma genes and core pathways. Nature. 2008; 455:1061–1068. [PubMed: 18772890]
5. Druker BJ. Translation of the Philadelphia chromosome into therapy for CML. Blood. 2008; 112:4808–4817. [PubMed: 19064740]
6. Flaherty KT, et al. Inhibition ofmutated, activated BRAF in metastatic melanoma. N. Engl. J. Med. 2010; 363:809–819. [PubMed: 20818844]
7. Geyer CE, et al. Lapatinib plus capecitabine for HER2-positive advanced breast cancer. N. Engl. J. Med. 2006; 355:2733–2743. [PubMed: 17192538]
8. Boss DS, Beijnen JH, Schellens JH. Clinical experience with aurora kinase inhibitors: a review. Oncologist. 2009; 14:780–793. [PubMed: 19684075]

9. Haura EB, et al. A Phase II study of PD-0325901, an oral MEK inhibitor, in previously treated patients with advanced non-small cell lung cancer. Clin. Cancer Res. 2010; 16:2450–2457. [PubMed: 20332327]
10. LoRusso PM, et al. Phase I pharmacokinetic and pharmacodynamic study of the oral MAPK/ERK kinase inhibitor PD-0325901 in patients with advanced cancers. Clin. Cancer Res. 2010; 16:1924–1937. [PubMed: 20215549]
11. Knight ZA, Lin H, Shokat KM. Targeting the cancer kinome through polypharmacology. Nature Rev. Cancer. 2010; 10:130–137. [PubMed: 20094047]
12. Karaman MW, et al. A quantitative analysis of kinase inhibitor selectivity. Nature Biotechnol. 2008; 26:127–132. [PubMed: 18183025]
13. Mestres J, et al. The topology of drug-target interaction networks: implicit dependence on drug properties and target families. Mol. Biosyst. 2009; 5:1051–1057. [PubMed: 19668871]
14. Wilhelm S, et al. Discovery and development of sorafenib: a multikinase inhibitor for treating cancer. Nature Rev. Drug Discov. 2006; 5:835–844. [PubMed: 17016424]
15. Ahmad T, Eisen T. Kinase inhibition with BAY 43-9006 in renal cell carcinoma. Clin. Cancer Res. 2004; 10:6388S–6392S. [PubMed: 15448036]
16. Lairmore TC, et al. A 1.5-megabase yeast artificial chromosome contig from human chromosome 10q11.2 connecting three genetic loci (*RET, D10S94*, and *D10S102*) closely linked to the *MEN2A* locus. Proc. Natl Acad. Sci. USA. 1993; 90:492–496. [PubMed: 8093642]
17. Almeida MQ, Stratakis CA. Solid tumors associated with multiple endocrine neoplasias. Cancer Genet. Cytogenet. 2010; 203:30–36. [PubMed: 20951316]
18. Read RD, et al. A *Drosophila* model of multiple endocrine neoplasia type 2. Genetics. 2005; 171:1057–1081. [PubMed: 15965261]
19. Vidal M, et al. ZD6474 suppresses oncogenic RET isoforms in a *Drosophila* model for type 2 multiple endocrine neoplasia syndromes and papillary thyroid carcinoma. Cancer Res. 2005; 65:3538–3541. [PubMed: 15867345]
20. Wells SA Jr, et al. Vandetanib in patients with locally advanced or metastatic medullary thyroid cancer: a randomized, double-blind Phase III trial. J. Clin. Oncol. 2012; 30:134–141. [PubMed: 22025146]
21. Hinz U, Giebel B, Campos-Ortega JA. The basic-helix-loop-helix domain of *Drosophila* lethal of scute protein is sufficient for proneural function and activates neurogenic genes. Cell. 1994; 76:77–87. [PubMed: 8287481]
22. Wilhelm SM, et al. BAY 43-9006 exhibits broad spectrum oral antitumor activity and targets the RAF/MEK/ERK pathway and receptor tyrosine kinases involved in tumor progression and angiogenesis. Cancer Res. 2004; 64:7099–7109. [PubMed: 15466206]
23. Sun L, et al. Discovery of 5-[5-fluoro-2-oxo-1,2- dihydroindol-(3Z)- ylidenemethyl]-2,4-dimethyl-1H-pyrrole-3-carboxylic acid (2-diethylaminoethyl)amide, a novel tyrosine kinase inhibitor targeting vascular endothelial and platelet-derived growth factor receptor tyrosine kinase. J. Med. Chem. 2003; 46:1116–1119. [PubMed: 12646019]
24. Dar AC, Lopez MS, Shokat KM. Small molecule recognition of c-Src via the imatinib-binding conformation. Chem. Biol. 2008; 15:1015–1022. [PubMed: 18940662]
25. Vidal M, Larson DE, Cagan RL. Csk-deficient boundary cells are eliminated from normal *Drosophila* epithelia by exclusion, migration, and apoptosis. Dev. Cell. 2006; 10:33–44. [PubMed: 16399076]
26. Read RD, Bach EA, Cagan RL. *Drosophila* C-terminal Src kinase negatively regulates organ growth and cell proliferation through inhibition of the Src, Jun N-terminal kinase, and STAT pathways. Mol. Cell. Biol. 2004; 24:6676–6689. [PubMed: 15254235]
27. Vidal M, et al. Differing Src signaling levels have distinct outcomes in *Drosophila*. Cancer Res. 2007; 67:10278–10285. [PubMed: 17974969]
28. Sawamoto K, et al. The *Drosophila* secreted protein Argos regulates signal transduction in the Ras/MAPK pathway. Dev. Biol. 1996; 178:13–22. [PubMed: 8812105]
29. Guichard A, et al. *rhomboid* and *Star* interact synergistically to promote EGFR/ MAPK signaling during *Drosophila* wing vein development. Development. 1999; 126:2663–2676. [PubMed: 10331978]

30. Gedaly R, et al. PI-103 and sorafenib inhibit hepatocellular carcinoma cell proliferation by blocking Ras/Raf/MAPK and PI3K/AKT/mTOR pathways. Anticancer Res. 2010; 30:4951–4958. [PubMed: 21187475]

31. Carracedo A, et al. Inhibition of mTORC1 leads to MAPK pathway activation through a PI3K-dependent feedback loop in human cancer. J. Clin. Invest. 2008; 118:3065–3074. [PubMed: 18725988]

32. Carlomagno F, et al. ZD6474, an orally available inhibitor of KDR tyrosine kinase activity, efficiently blocks oncogenic RET kinases. Cancer Res. 2002; 62:7284–7290. [PubMed: 12499271]

33. Alon U. Network motifs: theory and experimental approaches. Nature Rev. Genet. 2007; 8:450–461. [PubMed: 17510665]

34. Brachmann CB, et al. The *Drosophila* Bcl-2 family member dBorg-1 functions in the apoptotic response to UV-irradiation. Curr. Biol. 2000; 10:547–550. [PubMed: 10801447]

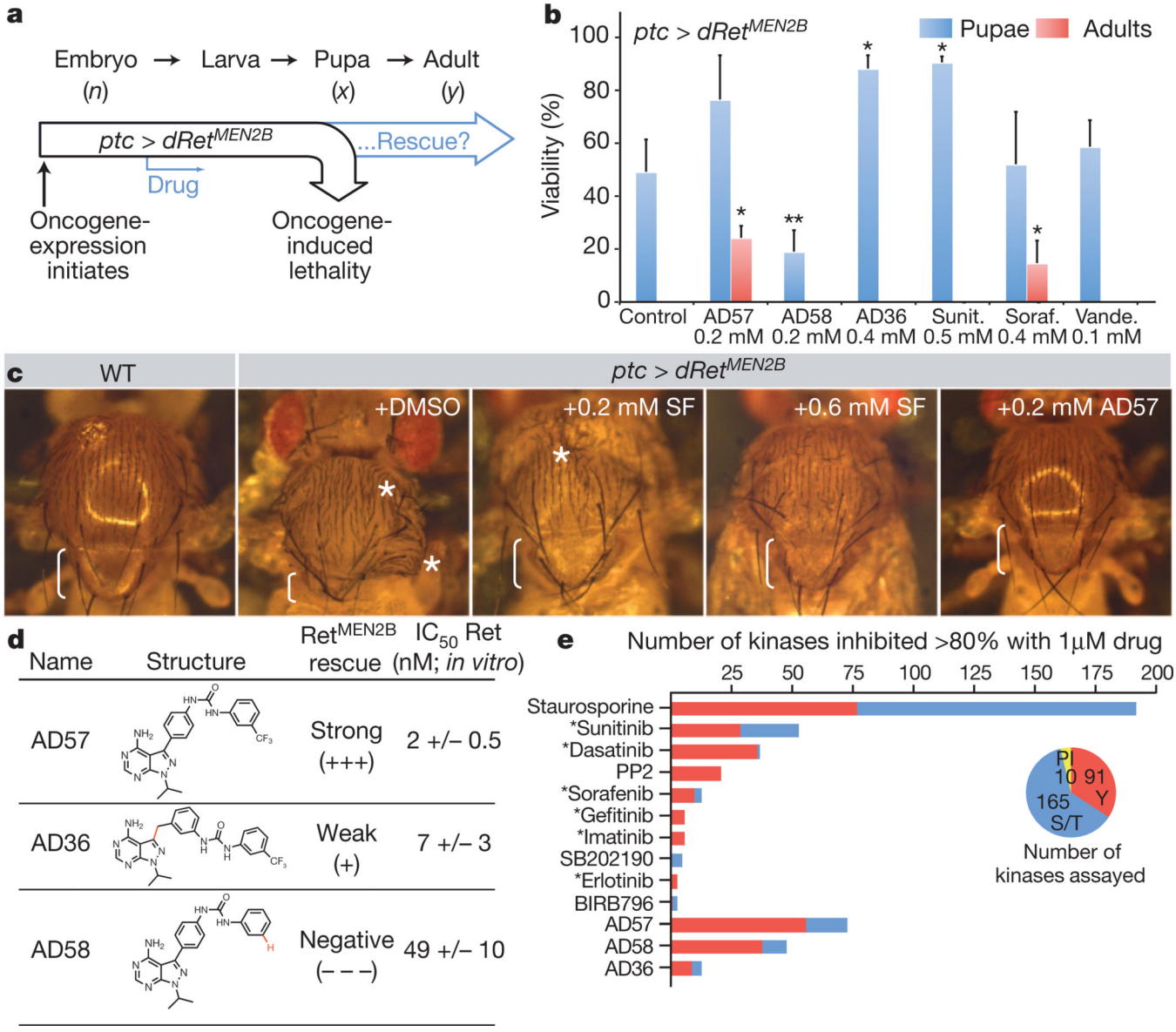

Figure 1. Screening for an optimal therapeutic index in a *Drosophila* MEN2B model yields a polypharmacological kinase inhibitor

a, Suppression of dRet^{MEN2B}-induced developmental block and whole-animal toxicity were scored based on the number of embryos (*n*) that survived as pupae (*x*) and adults (*y*). **b**, Per cent viability of control- or drug-treated flies determined for pupae (*x* per *n*) and adults (*y* per *n*). AD57 emerged as the best single-agent hit from the screen. Asterisks indicate significance comparing to control using Student's *t*-test ($P < 0.05$ for adults in AD57 and sorafenib treatments, and $P < 0.05$ for pupae for the rest). Error bars denote s.e.m. Total *n* of 200, 75, 98, 54, 91, 280 and 209, from left to right. Soraf., sorafenib; Sunit., sunitinib; Vande., vandetanib. **c**, *ptc > dRet^{MEN2B}* adults have notum defects including excessive bristles (asterisks) and scutellum defects (brackets); controls (+ dimethylsulphoxide (DMSO)) died as un-eclosed adults. AD57 strongly suppressed whereas sorafenib (SF) weakly suppressed these defects, yielding fully eclosed adults. Width of each wild-type notum is ~0.75 mm. WT, wild type. **d**, Structure–activity relationships suggest that dRet inhibition alone is insufficient to rescue MEN2B flies. IC_{50} values were determined against

a purified form of human Ret. **e**, The AD series of compounds showed broad-spectrum kinase-inhibition profiles. Clinical (asterisks) and known kinase inhibitors are shown for comparison. The number of lipid (PI), tyrosine (Y) and serine/threonine (S/T) kinases tested are shown in the pie chart.

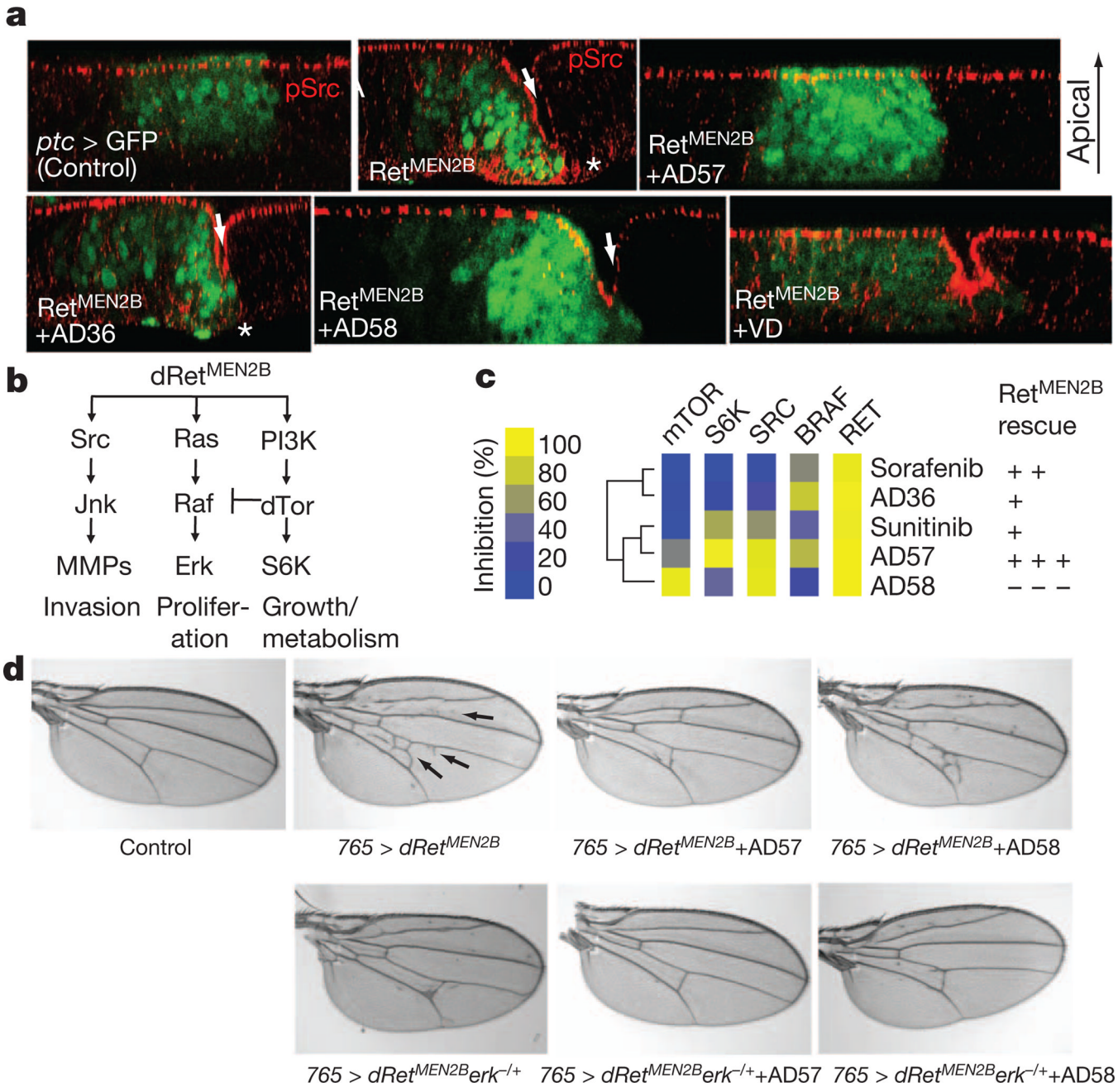

Figure 2. Multiple-pathway inhibition by AD57 mitigates dRet-directed phenotypes

a, z-series confocal images of larval wing epithelia; virtual cross-section through tissue with apical up. Control tissue shows apical phospho-Src (pSrc) expression (red) in the junctions. *ptc > dRet*^{MEN2B} wing cells (green fluorescent protein; GFP^{+}) shifted basally (arrows) and invaded below adjacent wild-type tissue; phospho-Src emerged at the basal invading front (asterisks). These phenotypes were strongly suppressed by AD57 but not by AD36, AD58 or vandetanib (VD). Apical–basal distance is ~45 μm; imaged with ×63 oil. **b**, Partial list of signalling pathways activated by oncogenic dRet^{MEN2B}. MMPs, matrix metalloproteinases. **c**, Per cent *in vitro* kinase inhibition profiles (left) and relative rescue (right) are shown. Tree indicates similarity of compounds on the basis of hierarchical clustering of per cent kinase inhibition. **d**, Broad dRet^{MEN2B} expression led to ectopic wing veins (arrows), reflective of

hyperactive Ras pathway signalling. The wing defects were suppressed by AD57 and enhanced by AD58. Removal of one functional copy of *erk/rolled* (*erk*$^{-/+}$) enhanced rescue by AD57 and AD58. Quantified in Supplementary Figure 5c.

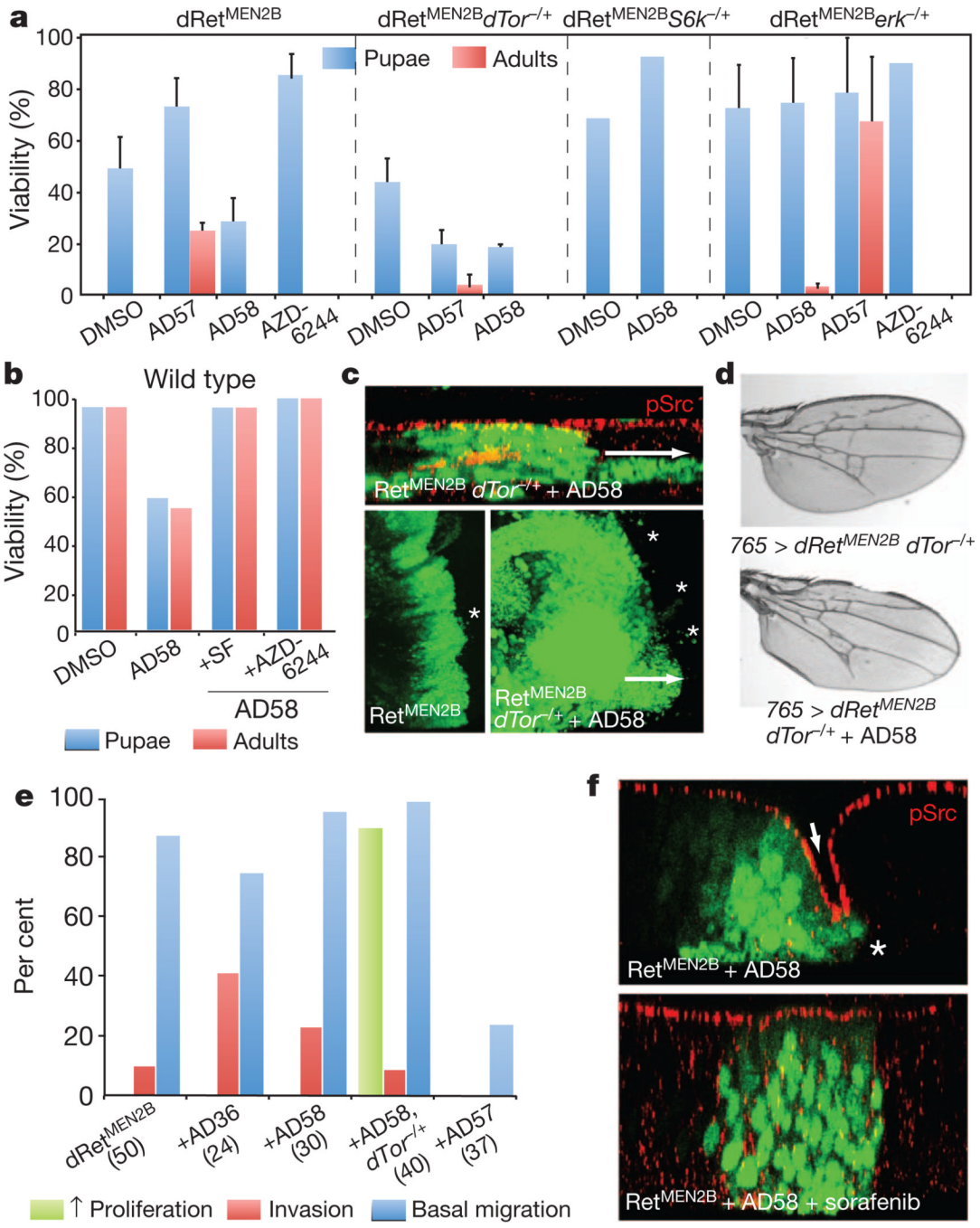

Figure 3. Feedback downregulation of the Ras pathway through the anti-target Tor

a, Reducing *dTor* gene dosage decreased per cent viability of AD57- nd AD58-treated dRet^{MEN2B} flies ($P < 0.05$ comparing pupae (AD57, AD58) or adults (AD57)). Conversely, reducing *erk* gene dosage enhanced survival of both ($P < 0.05$ comparing pupae (AD58) or adults (AD57)). Treatment with a specific MEK inhibitor alone, AZD6244, in control (*ptc > dRet^{MEN2B}*) or *erk*$^{-/+}$ flies did not rescue viability compared to AD57-treated flies, suggesting its level of Ras pathway suppression is close to optimal (P>0.05 comparing AZD6244 pupae). Reducing S6K (*S6k*$^{-/+}$) partially mitigated toxicity from AD58 treatment. Column bars represent the mean of three separate experiments. Total n of 214, 58, 63, 130, 254, 66, 118, 52, 59, 190, 93, 114 and 96 from left to right. Error bars denote s.e.m. **b**,

Decreased viability of wild-type flies by AD58 was mitigated by co-administration of sorafenib or AZD6244. Total *n* of 118, 47, 51 and 28 from left to right. **c**, Reducing *dTor* strongly enhanced AD58-mediated invasion (asterisks, arrow) and excess proliferation. Top panel, a lateral reconstruction; compare with Fig. 2a. Bottom panels represent an apical view, constructed as a z-series overlay of confocal images spanning the full depth of the wing disc epithelia. It shows how cells migrate from the *ptc* domain to distant sites (for example, arrow, asterisks), a phenotype strongly enhanced in the presence of $dTor^{-/+}$ plus AD58. Top panel (GFP+) width is ~150 μm; imaged with ×63. Bottom right panel width (GFP+) is ~150 μm; both bottom panels were imaged with ×40. **d**, Wing defects in *ptc* > $dRet^{MEN2B}$ $dTor^{-/+}$ adults were further enhanced by AD58. **e**, Quantification of *ptc* > $dRet^{MEN2B}$ phenotypes. Invasion was established by scoring for single or groups of GFP-labelled cells that relocated away from the *ptc* boundary (Fig. 3c, asterisks). Basal migration was scored as indentation of the apical surface (see Fig. 2a, arrows). Proliferation was scored as significant widening of the *ptc* boundary. The number of wings analysed under each condition is indicated in brackets. Reduced *dTor* increased proliferation in the presence of AD58 as well as reducing survival; all aspects were improved by feeding AD57 whereas increased invasion by feeding AD36 did not translate to reduced survival. **f**, Migration of $dRet^{MEN2B}$-transformed cells was blocked by co-treatment with AD58 plus sorafenib (bottom). Treatment with similar doses of AD58 (top) or sorafenib alone (not shown) did not suppress migration. Arrow indicates constriction of apical cell surface and asterisk indicates basal invading front. Apical–basal distance is ~45 μm; imaged with ×63.

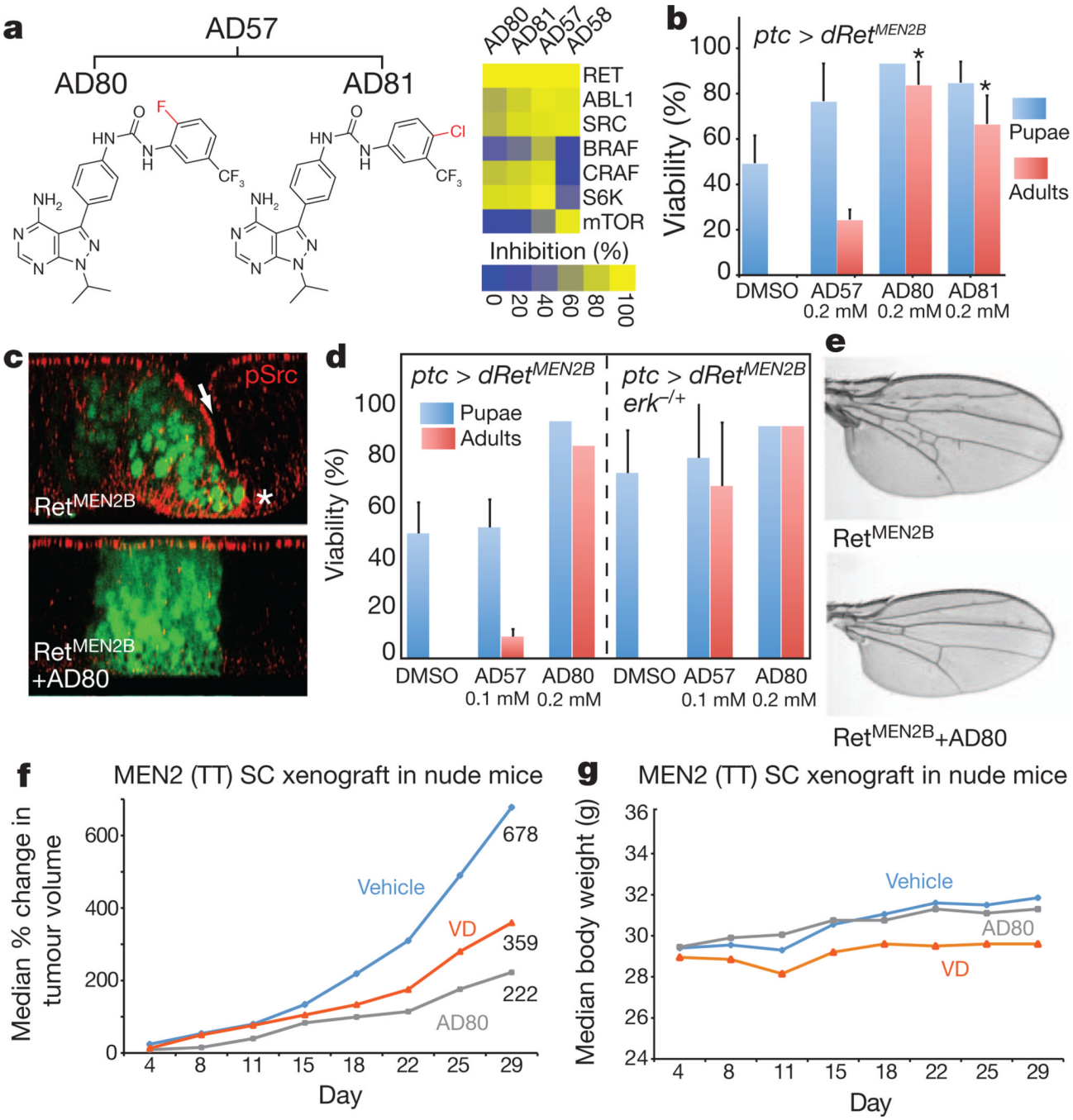

Figure 4. Balanced kinase polypharmacology provides optimal efficacy and toxicity

a, Chemical structures of the AD57 derivatives AD80 and AD81 and percentage inhibition of relevant targets at 1 μM. Unlike AD57 and AD58, both lack significant inhibitory activity against mTOR. **b**, AD80 and AD81 showed improved rescue relative to AD57. *$P < 0.05$, significance compared to AD57 in a two-tailed Student's *t*-test. Total *n* of 214, 58, 109 and 99 from left to right. Error bars denote s.e.m. **c**, Basal migration (arrow) of dRet^{MEN2} cells and basal phospho-Src (pSrc; asterisk) were blocked by AD80. Apical–basal distance is ~45 μm; imaged with ×63. **d**, Reducing *erk* gene dosage enhanced survival of AD57 ($P < 0.05$ for adult flies compared across genotypes) but not AD80 ($P > 0.5$ for adults compared across

genotypes), suggesting that the Tor feedback loop was not altered by AD80 and that Erk was optimally suppressed in flies. Total *n* of 214, 43 and 109 from left to right. Error bars denote s.e.m. **e**, *765 > dRet*^{MEN2B}-dependent extra wing vein phenotype was fully rescued by AD80. **f**, AD80 and vandetanib (VD) reduced tumour progression 3.1- and 1.9- fold, respectively, relative to vehicle-treated nude mice transplanted with TT cells. Change in tumour volume was calculated per mouse and shown are the median per group. Twenty vehicle- and ten drug-treated mice were analysed for each treatment group. **g**, Corresponding body-weight measurements.

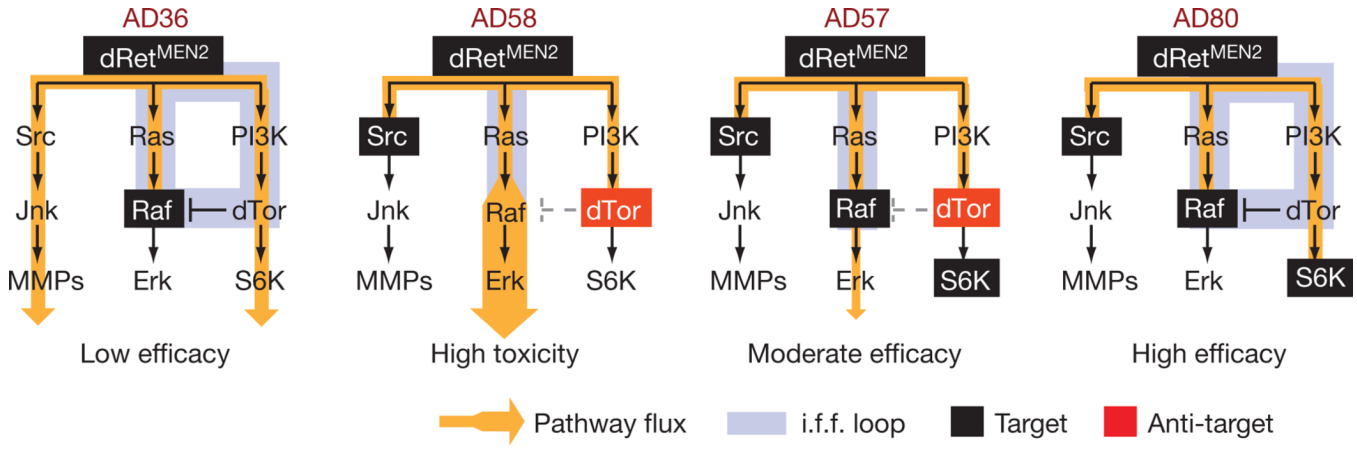

Figure 5. Differential polypharmacology and outcomes from the AD compounds

Models to explain the AD series of compounds in dRet^{MEN2B} transgenic flies. Pathway components blocked by inhibitors have been boxed, with resulting flux indicated by orange lines and arrows, and the incoherent feed-forward (i.f.f.) loop highlighted in blue. Grey dashed lines indicate loss of dTor inhibition. Targets in black boxes contribute to efficacy whereas inhibition of the anti-target dTor (red) leads to hyperactivation of the Ras pathway, causing high toxicity in the MEN2 model. The polypharmacological profile of AD80 best addresses the three key pathways, providing high drug efficacy and optimal therapeutic index.